Journal of Applied Polymer Science

Role of silk fibroin and rice starch on some physical properties of hydroxyapatite-based composites

Suchaya Sriudom,[1] Hataichanoke Niamsup,[2] Surin Saipanya,[2] Ruangsri Watanesk,[1] Surasak Watanesk[1]

[1]Department of Chemistry, Materials Science Research Center and Center of Excellence for Innovation in Chemistry, Faculty of Science, Chiang Mai University, Chiang Mai, Thailand

[2]Department of Chemistry and Materials Science Research Center, Faculty of Science, Chiang Mai University, Chiang Mai, Thailand

Correspondence to: S. Watanesk (E-mail: swatanes@gmail.com)

ABSTRACT: The role of organic blends of silk fibroin (SF) and rice starch (RS) in bone composites based on inorganic hydroxyapatite (HA) is studied. The physical property of HA-based composites prepared by using the sol–gel method from $Ca(OH)_2$ and H_3PO_4 in ethanol and water solvent (4 : 1 volume ratio) could be improved by adding SF and RS (1 : 2 weight ratio) to HA (7 : 3 weight ratio). The Fourier transform infrared spectrometer spectrum shows that the SF and RS organic phases are blended homogeneously into the HA crystal structure. Addition of SF increases the pore size and surface area of the composites, as measured by Brunauer–Emmett–Teller method, but their pore volume is slightly decreased. The values of lattice parameters, crystallinity, and crystallite size, as determined from the field-emission scanning electron microscope, transmission electron microscope, and X-ray diffractometer results, increase after adding RS. The results are agreeable with the increase of their compressive strength and Young's modulus. Thus, the improved physical property of the prepared HA–SF/RS composites is better suited as bone-filling material than the standard HA or HA-based composites with either SF or RS only. Therefore, due to its low cost, biocompatibility, and nontoxicity, this innovative solution could be worth taken under consideration by the restorative dental and orthopedic implants industry. © 2015 Wiley Periodicals, Inc. J. Appl. Polym. Sci. **2015**, *132*, 42722.

KEYWORDS: biomaterials; composites; nanoparticles; nanowires and nanocrystals

Received 26 February 2015; accepted 12 July 2015

DOI: 10.1002/app.42722

INTRODUCTION

Nowadays, people are increasingly turning their attention to health care. Aging people normally have calcium-loss problem together with the decrease of collagen production and there is less growth hormone produced. In the end, the bones become brittle and susceptible to fracture. Sometimes, following an accident or removal of tumor, gaps in fractured bones need to be filled if a section of bone is missing. Thus, there is considerable demand for bone substitutes. And good bone replacing materials have been a matter of quest in bone surgery for decades. Normally, natural bone and teeth consist of two major components: organic and inorganic (or mineral) phases. The inorganic phase is a special form of calcium phosphate, $Ca_{10}(PO_4)_6(OH)_2$, commonly called hydroxyapatite (HA). Usually, it represents about 70% of the bone's weight. While the remaining 30% is collagen, the organic phase, which supports crystal growth.

There are several options for carrying out bone replacement. Two of them, allografts and autografts, involve using bone from another and same patient, respectively. However, there are risks of infection and rejection of the implant. In addition, such bone is simply not strong enough. Therefore, synthetic materials are gradually becoming more popular and the use of synthetic HA has become the norm in orthopedics and dentistry. The key reason is its biocompatibility due to the chemical and biological similarity to the mineral phase of human bones and teeth.[1] Unfortunately, it is also too brittle to be used on its own for large-scale applications. Thus, composites of HA with degradable polymers are used, which resorb over time and allow bone to regrow and fill the space.

Until now, most of the prepared bone-replacing materials have been concentrated on using biopolymers for improving the mechanical properties of the HA-based composites. Some natural polymers used in bone reforming include collagen, chitosan, and alginate. They became valuable candidates for biomedical applications due to their good biocompatibility, noncytotoxicity, minimal inflammation, design flexibility as well as bone healing efficacy.[2] In addition to these biopolymers, silk fibroin (SF) is

another interesting biopolymer. It is derived from silk, a well-known natural fiber produced by silkworm, such as *Bombyx mori*. It has favorable mechanical properties, high oxygen permeability, and nontoxicity to tissue with its appreciable bioactivity similar to human skin. So, it has been used in making suture material, fabricating biosensors and nanofibers, and repairing bones and cartilages.[3]

In the last decade, many HA/SF nanocomposites were successfully prepared by various methods.[4] For example, Chunling *et al.*[5] fabricated composite films of *Bombyx mori* SF and HA. Their films were smooth and transparent with uniform distribution of HA. The HA crystals had anisotropic growth with high extent of lattice imperfection and preferential orientation along *c*-axis that were probably promoted by the addition of SF. But, regarding the bone requirements, the HA/SF composite may not be suitable as bone-replacing material due to its insufficient formability and flexibility.

Another promising natural material used in medical applications is rice starch (RS). RS is used to improve the mechanical properties of HA by promoting tissue healing and active bone formation.[6] Wheat starch is also used to combine with HA.[7] It has been shown that this biopolymer, as a template agent, has influence on the shape of HA. It led to the formation of rod-like HA, which is similar to this inorganic component in natural bone. It is expected that properties of the prepared nanocomposites are similar to those of the natural bone. From this result, the HA composites could be moderated in order to utilize its specific properties such as biocompatibility and biodegradability. Recently, Park *et al.*[8] made an approach on preparing a ternary composite of SF/nano-HA with corn starch. The capability of bone formation with this ternary composite scaffold as a bone defect replacement matrix when grafted in a calvarial bone defect of rabbits *in vivo* was evaluated. The rabbit calvarial defect was not successfully repaired, possibly due to an inflammatory reaction caused by silk powder.

In our previous work,[9] solvent composition for the preparation of HA/SF composites using sol–gel method were optimized. It was found that the optimal condition for preparing the composites was in an EtOH/H_2O medium at a volume ratio of 4 : 1. This condition was deducted from the data on their crystallinity, particle size distribution (PSD), particle size, surface morphology, and Ca/P ratio. However, the prepared composite had some disadvantages due to high crystallinity, modulus, and strength.

An enticing approach to improve our earlier composite's mechanical properties is to incorporate RS into the composite because the RS molecule itself is large and able to form gel. And, consequently, RS can improve mobility and flexibility of the composites. In this study, the procedure from our previous work[7] has been utilized again for preparing several HA-based composites with blended SF and/or RS. Then, important physical and mechanical properties of these composites were evaluated to determine the suitability of the composite as a bone-filling material. Some physical properties of the composites were evaluated expecting that these composites should possess a suitable average pore size, porosity, crystallinity, and mechanical properties that meet the requirement to be used as bone-filling materials.

Table I. Weight Ratio of the HA Compound and HA-Based Composites Used for Each Sample Preparation

Sample	Weight ratio of HA: SF: RS
HA	10 : 0 : 0
HA/SF	7 : 3 : 0
HA/RS	7 : 0 : 3
HA/SF-RS1	7 : 1 : 2
HA/SF-RS2	7 : 1.5 : 1.5
HA/SF-RS3	7 : 2 : 1

EXPERIMENTAL

Materials

SF was extracted from *B. mori* silk wastes (Nangnoi Srisaket 1), purchased from Queen Sirikit Sericulture Center, Chiang Mai province, Thailand. SF powder derived from silk waste was prepared as described by Moonsri *et al.*[10] RS (Era-Tab, 99%) was purchased from Erawan Pharmaceutical Research and Laboratory Co., Ltd, Thailand. Calcium hydroxide ($Ca(OH)_2$), orthophosphoric acid (H_3PO_4, 85%), ammonium hydroxide (NH_4OH), absolute ethanol (C_2H_5OH), and hydrochloric acid (HCl, 37%) were purchased from Merck, Germany. Potassium chloride (KCl, 99.5%) was purchased from Ajax Finechem, Australia. All other chemicals used in this study were of analytical grade. Deionized distilled water was used throughout the experiments.

Preparation of HA Compound and HA-Based Composites

A sol–gel method was used for preparing HA compound as well as the HA-based composites with SF and RS. The compositions of the HA and organic phases (SF and/or RS) were fixed at 70 : 30 weight ratio of HA: organic phase.

SF powder derived from silk waste was prepared as described by Moonsri *et al.*[10] The HA-based composites were prepared, as described by Sriudom *et al.*,[9] in a binary medium of EtOH/H_2O at 4 : 1 volume ratio. The pH of the mixed solution was adjusted to 9 by adding NH_4OH and stirred for 2 h to get the precipitate formed. The precipitate was aged at room temperature for 2 h, filtered and washed repeatedly using warm deionized distilled water. Then it was dried at 60°C for 24 h in an oven and, finally, pulverized. The resulting fine powder was stored in a desiccator. The composition of the prepared composites is shown in Table I.

Respective binary and ternary composites were prepared by mixing the HA solution with SF and/or RS at the following weight ratios (HA : SF : RS): 7 : 3 : 0, 7 : 0 : 3, 7 : 1 : 2, 7 : 2 : 1, and 7 : 1.5 : 1.5. The resulting HA-based composites were assigned as HA/SF, HA/RS, HA/SF-RS1, HA/SF-RS2, and HA/SF-RS3, respectively.

Preparation of Putty HA-Based Composites

Preparation of the putty composite was done by dropping 1 mL of 20% w/v aqueous citric acid solution into 1 g of HA-based

powder, then mixing by hand until homogeneous putty formed and, finally, molding it into a cylindrical shape (5.0 mm in diameter and 10.0 mm in length). Other putty HA-based composites were prepared in a similar fashion using different kinds of HA-based powder. Some physical properties of the putty composites were investigated.

CHARACTERIZATION OF THE HA COMPOUND AND HA-BASED COMPOSITES

Structure Conformation

Preliminary study and functional group analysis of the HA-based composites were done spectrometrically with a Fourier transform infrared spectrometer (FTIR) (Perkin Elmer, 1760) in the range of 4000–400 cm^{-1}.

Crystallinity

Crystallinity of the HA-based composites was characterized using a X-ray diffractometer (XRD) (Rigaku, Miniflex II) with a monochromatic radiation of CuKα ($\lambda = 1.54$ Å) over the 2θ range of 2(60°) at a scan rate of 6°/min. Identification of the crystalline phases was done by comparing the spectra with the stand powder diffraction card of Joint Committee on Powder Diffraction Standards (JCPDS) files to estimate the crystallite size in a perpendicular direction based on the Scherrer's formula as follows:[11]

$$D = 0.89\lambda/\beta\cos\theta \quad (1)$$

where D is the mean value of the crystallites size, λ is the X-ray emission wavelength, β is full width at half maximum for the diffraction peak of (002) under consideration (rad), and θ is the diffraction angle (°).

Crystal Phase

Ultrafine structures of the HA-based composites were examined by a transmission electron microscope (TEM) (JEOL, JEM 2010) at 200 kV. Upon preparing the samples for TEM analysis, the powder was ultrasonically dispersed in ethanol prior to being drop-casted onto a holey carbon supported film. The TEM spectrum was determined with a software using virtual standards for the Ca and P Kα X-ray peaks.

Particle Size Distribution

Particle size distribution (PSD) of all HA-based composites was measured using a particle size analyzer (Autosizer Lo-C; Malvern Instruments) to obtain a mean particle size of the seed particles. The composites had been dispersed in ethanol before PSD was determined. The shape of the distribution curve was of prime interest.

Particle Morphology

Morphology of the HA-based composites was determined using a field-emission scanning electron microscope (FE-SEM) (JEOL, JSM 6300 F). For SEM, the composites were spread on metal stubs and coated with gold before examination.

Density and Porosity Measurement

Bulk density of the putty composites was easily determined from the weights of the cylindrical samples. The pore volume was determined by immersing a dried cylindrical sample into a small beaker containing 50 mL deionized distilled water for 2 h until there was no air bubbling out of the sample to ensure water saturation of the cylindrical samples. Then, the cylindrical sample was removed from the beaker and reweighed. The porosity of the open pores was calculated using Archimedes' method.

Compressive Strength and Young's Modulus

Each of the putty HA-based composites was molded into a cylindrical shape. The compressive strength of the cylindrical samples was measured using a universal testing machine (Shimadzu, Autograph DSS-5000) at a crosshead speed of 0.5 mm/min. Young's modulus (E) was calculated from the recorded load-deflection curves.

Surface Area

Pore volumes of the HA-based composites were determined using a pore size analyzer (Beckman Coulter, SA 3100), while surface area was measured by the Brunauer–Emmett–Teller (BET) method based on N_2 adsorption technique.

RESULTS AND DISCUSSION

The role SF and RS played on the properties of different HA composites was studied through FT-IR spectra, mechanical properties, and composite morphology. The results are as follows:

Structural Characterization of the HA Compound and HA-Based Composites

From Figure 1, the spectra of HA and all composites are revealed in order to identify their major characteristic peaks and also show the evidence of any interaction that may occur among the compositions in the composites. So the HA compound exhibits intense IR bands at 565 and 604 cm^{-1} and at 1040–967 cm^{-1} representing the PO_4^{3-} group [Figure 1(a)].[12] This group normally exists in the crystalline state of the HA. Absorbed water band is relatively broad at 3500–3000 cm^{-1}, and a weaker peak appears at 645 cm^{-1}. The band at 3620 cm^{-1} is assigned to the stretching mode of the OH group. Moreover, the CO_3^{2-} group (from dissolved CO_2) forms a weak peak at 870 cm^{-1} with more intense peaks at 1415 and 1530 cm^{-1}.

The prominent bands of SF in this work [Figure 1(b)] that occur at 1630 cm^{-1} (amide I, C=O stretching), 1535 cm^{-1} (amide II, N–H bending), and 1239 cm^{-1} (amide III, C–H stretching) show the existence of such amide groups in the β-sheet conformation of SF.[13] While the RS shows a broad absorption band at 3268 cm^{-1} [Figure 1(c)] corresponding to stretching frequency of the –OH group, and a band at 2920 cm^{-1} attributed to C–H stretching vibration.[14] The strong absorption band at 1648 cm^{-1} confirms the presence of water molecule. The bands around 1413 and 1337 cm^{-1} are assigned to $-CH_2$ bending in plane and C–OH bending vibration, respectively. The band at 1149 cm^{-1} is due to C–O–C antisymmetric bridge stretching.[15]

Absorption bands in Figure 1(d) show a combination of characteristic bands of both HA and SF in the HA/SF composite. Likewise, Figure 1(e) also shows the combined characteristic bands of HA and RS when RS was added into the HA composite. Therefore, the prominent peaks of both components in each of the HA/SF and HA/RS composites appear to be at about the same position as in the respective individual spectrums of SF

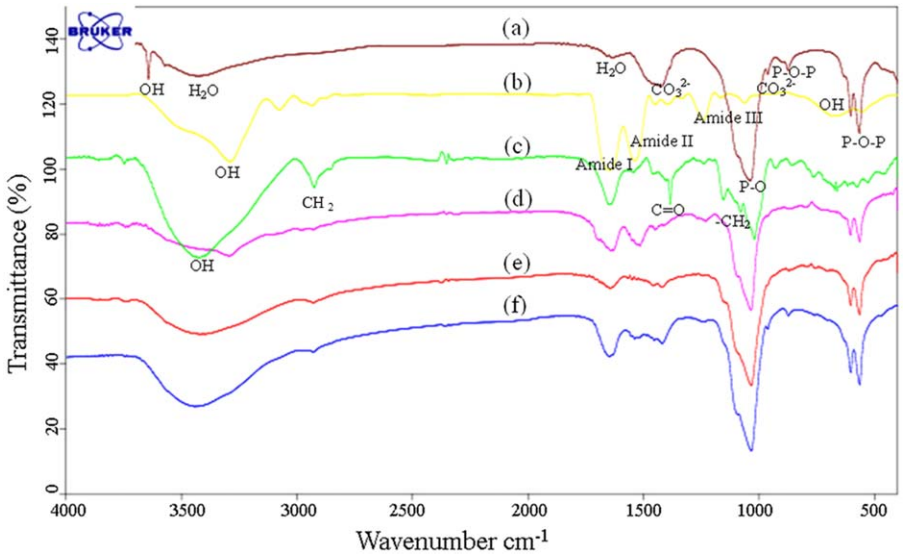

Figure 1. FTIR spectra of the (a) HA compound, (b) SF, (c) RS powders, (d) HA/SF, (e) HA/RS, and (f) HA/SF-RS composites. [Color figure can be viewed in the online issue, which is available at wileyonlinelibrary.com.]

and RS. Thus, it could be concluded that HA and organic phase physically blended without any significant chemical interaction between characteristic groups of each component.

Finally, when HA, SF, and RS are combined together in the ternary composite, each component still retains its typical peaks with only slight shifts [Figure 1(f)] as a result of dissociation and interaction of SF and RS with the nucleating crystals.[16] Moreover, some band overlapping of the RS and SF may cause the bands of amide II and amide III of SF to disappear. Also, as stated in some reports,[17] there are some chemical interactions between the inorganic and organic phases in the composite. Most likely between Ca^{2+} and those negatively charged functional groups in the organic matrix such as COO^{-}, amide I, and amide II. So for the absorption bands of HA/SF–RS composites, it happens that the overlapping of the OH^{-} group of RS and the -COOH group of SF turn out to be a board peak appearing in the range of 1750–1100 cm^{-1}. Thus, the presence of SF and RS molecules in the HA/SF–RS composites leads to the decrease of band intensities at 1647, 1538, 1242, and 1458 cm^{-1} as a result of intermolecular hydrogen bond formation between SF and RS molecules.

Crystallinity and Crystalline Size of the HA Compound and HA-Based Composites

From the XRD patterns in Figure 2, each pattern shows that HA is the only important phase because the other components do not contribute any peak to the XRD pattern. The well-resolved characteristic peak with the highest intensity of HA was obtained at 2θ value of 31.77° corresponding to the 211 plane. The phase formed was pure and matched well with the standard pattern. The standard corresponding planes of HA (200, 102, 201, 211, 112, 300, 202, 130, 222, 132, 321, and 004) are observed for both, the HA compound and HA-based composites. The HA/SF and HA/RS binary composites do exhibit similar XRD patterns. This indicates that the addition of SF and RS into the HA moiety leads to low crystallinity and that SF and RS have no effect on changing the crystallographic structure of HA.

While diffraction peaks of the (211), (202), and (300) planes can be differentiated as three individual sharp peaks for the pure HA, only a broader peak appears in the ternary composite of HA/SF–RS. The broad peak normally implies that the size and crystallinity of the composites are small and low. However, the intensities of the peaks of HA/SF–RS composite tend to decrease and the peaks become broader with the increase of RS content. It can be suggested that increasing the amounts of RS causes the RS molecules to be inserted in the space of the HA/SF crystal structure, then push apart the stack of the particle, resulting in disorder of the peaks. Noting that in all diffraction patterns, the signals are defined and assigned only to the crystalline HA because no secondary phase can be detected, even in the samples containing relatively large amount of SF and RS. The values of crystallite size, crystallinity and lattice parameters of the HA compound, HA/SF, HA/RS, and HA/SF–RS composites are shown in Table II using Bragg's law and Scherer's equation.

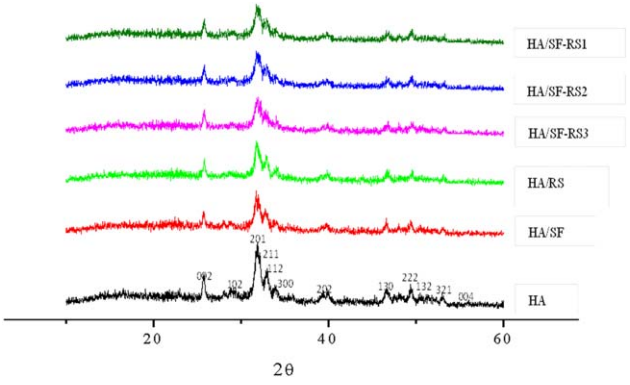

Figure 2. XRD patterns of the HA compound and HA-based composites. [Color figure can be viewed in the online issue, which is available at wileyonlinelibrary.com.]

Table II. Crystallite Size, Crystallinity, and Lattice Parameters of the HA Compound and HA-Based Composites

Sample	Crystallite size, X_s (nm)	Crystallinity, X_c (%)	Lattice parameters	
			a_0	c_0
HA	28.19 ± 2.06	93.35 ± 1.75	9.4071	6.8982
HA/SF	31.84 ± 2.12	92.69 ± 2.32	9.3989	6.8801
HA/RS	82.93 ± 2.53	93.13 ± 2.54	9.4422	6.9211
HA/SF-RS1	64.62 ± 3.45	65.93 ± 2.49	9.4255	6.9014
HA/SF-RS2	62.27 ± 2.96	82.01 ± 3.70	9.4133	6.8956
HA/SF-RS3	51.00 ± 2.72	88.10 ± 5.28	9.4088	6.8352

By determining the changes in lattice parameters of the HA composites and the shape of the crystallites, it was found that the composites consisted of hexagonal unit cells.[18] However, the FTIR result showed that the SF and RS did not induce conformational transformation of the HA crystal structure. This result also indicates the rearrangement of SF and RS molecules in the HA composite as it still retains its hexagonal structure due to the insertion of the organic molecules into the crystal structure. The calculated values of lattice parameters were found to be close to the standard HA with $a = b = 9.4180$ Å and $c = 6.8840$ Å. However, the lattice parameters have some changes with the change of RS content by increasing both a_0 and c_0. These are attributed to the crystal growth that causes the lattice strain by larger RS molecules. The RS molecules play a role by replacing the position of the smaller Ca atoms in the HA lattice, thus causing high compressive strength of the lattice. While SF can physically interact with HA in random, so the inclusion of the SF and RS makes the HA/SF–RS crystal formation incomplete. However, the HA formed as a ternary composite in this report is still in the desired Ca/P molar ratio value that conformed with the natural HA.

Crystal Phase of the HA Compound and HA-Based Composites

Since TEM allows a qualitative understanding of the internal structure of HA-based composites, it was used to analyze the crystal phase of the composite in order to see how the components were blended. Figure 3 shows the TEM images of the HA-based composites, the alignment of well-developed HA crystallites are illustrated and the interplanar spacing values were calculated from Bragg's diffraction equation. The calculated results indicate the fringe spacing is agreeable with the separation lattice planes of hexagonal phase. The crystal lattices were calculated from d-spacing using a selected area electron diffraction (SAED) pattern with a camera constant of 100 cm. The crystal planes of HA-based composites were obtained from the d-spacing values and compared against the JCPDS standards of HA. The electron diffraction in Figure 3(a) of the HA compound shows strongly focused spots which indicates strongly preferred (211) and (002) orientation of the HA crystals. The small particles cause the widening of many diffraction spots which can be noticed that their composite particles are mostly polycrystalline. From Figure 3(b,c), the (212) plane appears when either SF or RS is present in the HA binary composites, all nanoparticles showed uniform lattice fringes, meaning that no amorphous product was formed. This behavior can be attributed to the nucleation, growth, and aggregation of small particles with disordered surface in the plane by the SF and RS molecules.[17]

From the TEM images of the HA/SF–RS composites in Figures 3(d–f) with various composition ratios of SF and RS, the presence of composite crystallite size as nanoparticles can be confirmed. Those rings are indexed to be corresponding to (111), (212), and (003) planes of HA which have a hexagonal close packed (hcp) structure (JCPDS file no. 9-423). Thus, the HA particles were analyzed by TEM in detail, and all nanoparticles showed uniform lattice fringes, meaning that no amorphous product was formed.

Particle Size Distribution of the HA Compound and HA-Based Composites

In Figure 4, the HA compound shows a wider range of PSD compared to the HA/SF and HA/RS composites at the same weight ratio of 7 : 3. In the presence of SF, its molecule can be hydrolyzed resulting in a smaller molecular size than the RS molecule. Thus, the SF molecules can be easily included in the HA crystal formation. Therefore, when RS, a larger molecule, is added into the binary mixture, physical interactions through attraction by the functional groups of these components would cause agglomeration and precipitation of the composite. Once the HA is mixed with the SF and RS molecules which contain $-NH_2$ and COO^- groups, these groups will interact with Ca^{2+} and PO_4^{3-} through the sol–gel process.

By considering the PSD of the ternary composites (HA/SF–RS), particle size range of the HA/SF–RS composites is shorter than that of the HA compound. After the RS molecules are added into the HA/SF mixed solution, the COO^- group of the RS can be bound to Ca^{2+} and some amino groups of the SF, then the RS molecules are included into the HA crystal formation. Two ranges of PSD were found in all HA/SF–RS composites because of the effect of having SF and RS molecules in the ternary composites. The observed results may be explained by the fact that the RS molecule itself is large which allows easier agglomeration with Ca^{2+} to form the crystal structure. When the HA and SF molecules physically interact with each other, it is difficult for RS molecule which has a larger size to agglomerate thus causing the binary composite of HA/SF to have an appropriately small size range.

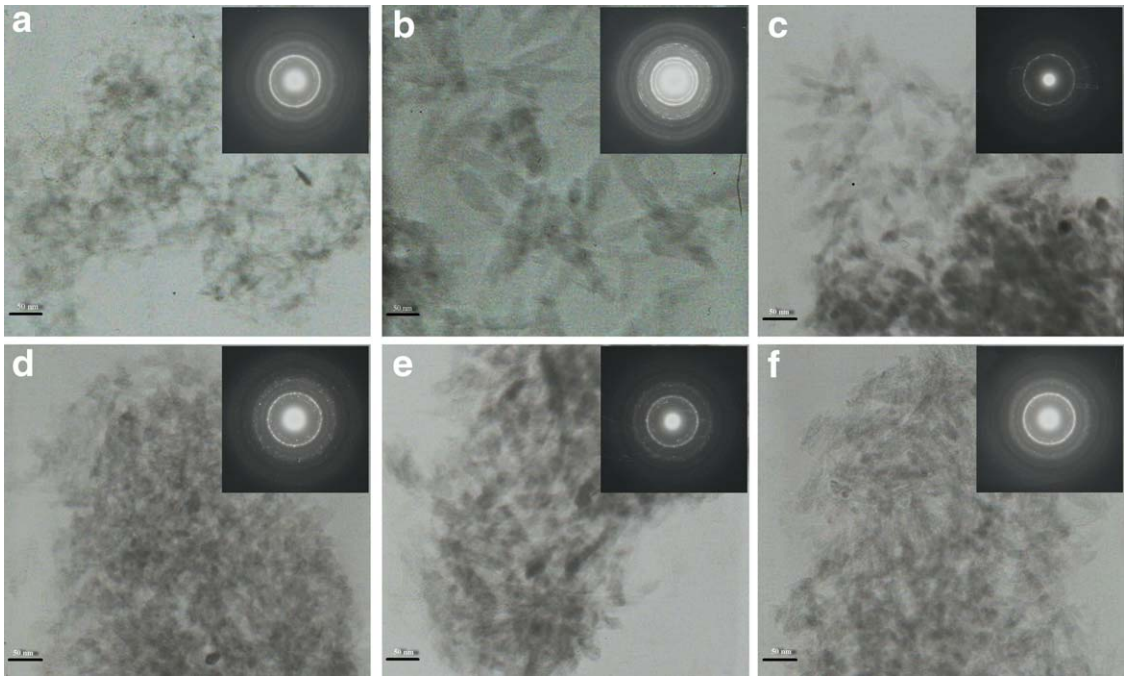

Figure 3. TEM images and its SAED pattern of the (a) HA compound, (b) HA/SF composites, (c) HA/RS composites, (d) HA/SF-RS1, (e) HA/SF-RS2, and (f) HA/SF-RS3 composites. [Color figure can be viewed in the online issue, which is available at wileyonlinelibrary.com.]

Particle Morphology of the HA Compound and HA-Based Composites

SEM images of the HA-based composites prepared using various compositions are seen through Figure 5. Particle size of the HA/RS (100–120 nm) is clearly larger than those of the HA/SF (74–85 nm) and HA (80–90 nm). However, micrographic results of the ternary HA-based composites show that its particle size is smaller than those of the binary HA-based composites and HA compound. The particle sizes of the ternary HA-based composites are 20–35 nm for HA/SF-RS3, 35–50 nm for HA/SF-RS2, and 60–80 nm for HA/SF-RS1.

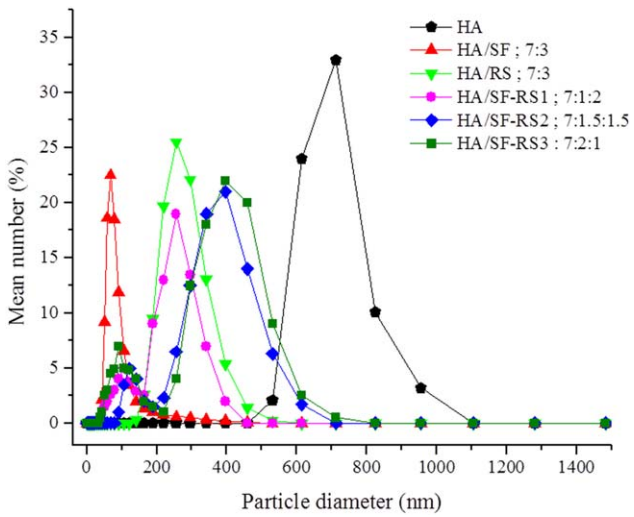

Figure 4. Particle size distribution of the HA compound, HA/SF, HA/RS, HA/SF-RS1, HA/SF-RS2, and HA/SF-RS3 composites. [Color figure can be viewed in the online issue, which is available at wileyonlinelibrary.com.]

The particle shape and chemical composition of the composite after the addition of an organic phase are thus expected to pose some effects on the mechanical properties of the composites. As being indicated that the biologic HA crystals are hexagonal with rice-grain-liked shape,[19] upon observing the shape of composite particle in our experiment, it can be seen that, at low content of RS, less particles with rice-grain-liked shape are formed. From this result, the nucleation and growth of the rice-grain-shaped crystal could be explained by the involvement of the crystals with different shapes at different concentrations of OH^- in the solution. This kind of involvement determined the growth rate and morphology of the crystals. The effect of OH^- content in the solution on the formation of the composite particles was also mentioned[20] in the way that Ca^{2+} could react with OH^- as well as PO_4^{3-} in the same direction along the axes which results in inducing the growth of crystal to be a rice-grain shaped. Since the amount of OH^- in the solution is affected by the presence of SF that its acidic functional group can react with the OH^-, so higher amount of RS (less amount of SF) would result in higher amount of OH^- left, thus producing more rice-grain-liked particles.

Compressive Strength and Young's Modulus of the Putty HA-Based Composites

The compressive strength and Young's modulus of the putty HA-based composites can be calculated from their forces and areas, and they are summarized in Table III.

The result indicates that the HA compound has the lowest compressive strength (0.38 MPa), which means that it is very brittle

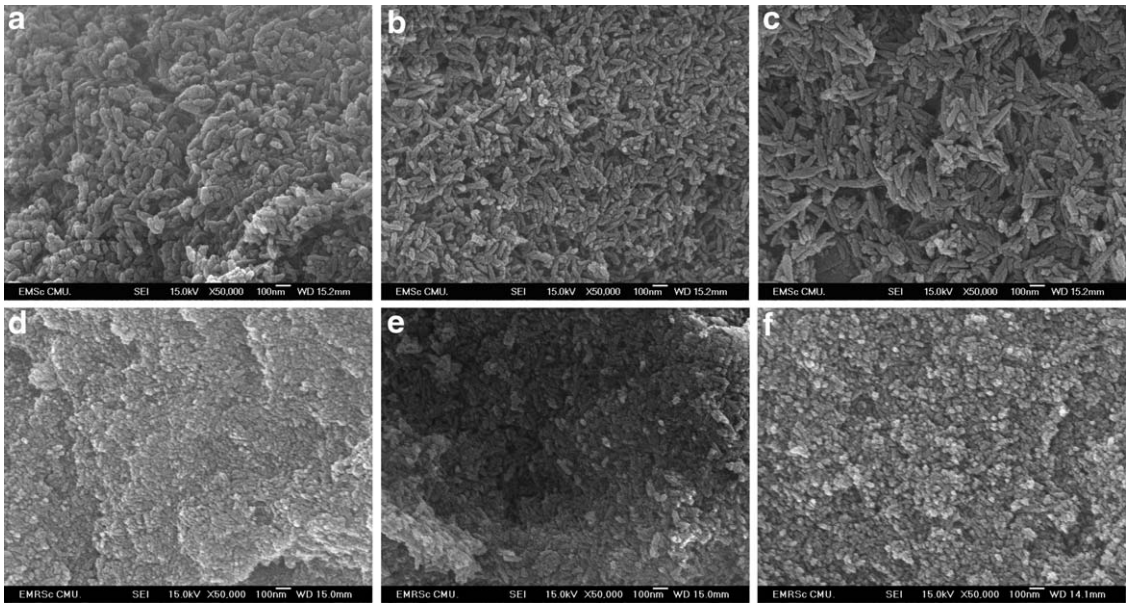

Figure 5. SEM images of the (a) HA compound, (b) HA/SF, (c) HA/RS, (d) HA/SF-RS1, (e) HA/SF-RS2, and (f) HA/SF-RS3 composites.

Table III. Compressive Strength and Young's Modulus of the Putty HA-Based Composites

Sample	Compressive strength (MPa)	Young's modulus (GPa)
HA	0.38	10.14
HA/SF	0.67	15.52
HA/RS	1.53	13.23
HA/SF-RS1	7.24	25.14
HA/SF-RS2	3.55	20.21
HA/SF-RS3	2.79	20.14

material. For the putty binary composites with the addition of organic phase, the HA/SF and HA/RS show higher values of the compressive strength. The organic phase causes the increase of the compressive strength and Young's modulus due to the fact that partial section of the composites suffered tension when HA/organic composites were mixed. For the ternary HA-based composites, the average values of compressive strength and Young's modulus drastically decrease with the increase of RS content. From the results, during composite preparation, the RS molecules induce absorption of excess water into the starch granule, thus make it swell during gelatinization. Back bone chains of amylose and amylopectin or their glucosidic linkages are postulated to lead to breakage of granular form causing reduction of the mechanical properties of the composites.[21]

Density and Porosity of the Putty-Liked HA-Based Composites

The porosity and density of the HA and its composites with SF and RS are shown in Table IV. From Table IV, for the putty binary composites, their porosity increases slightly compared to that of the HA compound when SF and RS are added. In the case of the putty ternary composites, HA/SF–RS, when more RS is added into the HA solution, more particles with rice grain shape is formed. As each particle agglomerates to form crystal, its rice-grain-shaped particle would become entangle due to the steric effect. This will result in a loose HA crystal formation causing it to be low in density but high in porosity as appeared in the Table IV when more RS is present. However, as the globular shaped crystal would form when more SF is present, at certain combinations of RS and SF contents, the globular shaped crystal could enter into the pore of the entangled rice-grain-

Table IV. Porosity, Density, Surface Area, Pore Volume, Surface/Volume, and Pore Size of the HA Compound, and Putty HA-Based Composites

Samples	Porosity (%)	Density $(g/cm)^3$	Surface volume (mm^3/g)	Pore volume (mm^3/g)	Surface/volume (mm^2/mm^3)	Pore size (nm)
HA	14.65 ± 0.56	1.825 ± 0.019	68.28	38.32	1.782	128.5
HA/SF	17.82 ± 0.84	1.641 ± 0.021	95.75	35.46	2.690	179.8
HA/RS	23.88 ± 0.10	1.695 ± 0.005	87.87	33.98	2.568	168.4
HA/SF-RS1	71.63 ± 0.72	1.185 ± 0.014	89.83	40.56	2.069	131.3
HA/SF-RS2	60.68 ± 1.25	1.341 ± 0.003	83.95	39.83	2.555	165.6
HA/SF-RS3	51.11 ± 0.77	1.476 ± 0.007	83.51	34.92	2.391	263.5

Table V. Summary of Bone-Filling Material Requirement

Requirement	Std. HA[22,23]	HA-based composites		Reference
		HA	HA/SF-RS1	
Particle size (nm)	50–100	50–100	50–100	50–80[24]
Crystal system	Hexagonal	Hexagonal	Hexagonal	Hexagonal[25]
Ca/P ratio	1.67	1.60	1.62	1.71[25]
Space group	P_{63}/m	P_{63}/m	P_{63}/m	P_{63}/m[25]
% Porosity	75–85	14.65	71.63	82.30[24]
Pore size (nm)	100–500	218.5	131.3	203[24]
Compressive strength (MPa)	5–60	0.38	7.24	5–30[26]
Young's modulus (GPa)	14–20	10.14	25.14	11–17[27]
Density (g/cm^3)	0.35–1.35	1.83	1.19	0.63–1.1[28]

shaped particle. Thus it will cause the porosity to be reduced, while the density of the crystal is enhanced.

Surface Area of the Putty HA-Based Composites

Specific surface area and particle size of the putty HA-based composites and the size of the powder particles were determined by BET theory. The BET surface area and total pore volume of the HA-based composites are summarized in Table IV.

Regulation of the pore structure (pore volume, pore size, and surface area) of the putty composite was demonstrated through controlling the contents of SF and RS in the HA solution. Moderately mixing of the SF and RS in the HA solution increases the surface area and pore volume, whereas the addition of more SF and RS do not significantly affect the pore volume of the putty composites. Moreover, significant addition of SF and RS to the HA solution reduces the average pore size and contributes to the formation of nanoporous structure. Generally, the pore volume of the binary composites are larger than that of the HA compound. It is notable that the maximum pore volume is observed for the composite of HA/SF–RS1 with a value of 40.56 mm^3/g. In addition, the HA/SF–RS2 and HA/SF–RS3 composites exhibit loose assembly of aggregated sphere-liked particles to form rice-grain-liked particles of which the surface area and pore volume are about 83.95 m^2/g, 83.51 m^2/g and 39.83 mm^3/g, 34.92 mm^3/g, respectively. The pore sizes of the putty composites, prepared using different composition ranges of HA, SF, and RS, are between 128.5 and 263.5 nm which indicate that the material is dominated by porous structure. Comparing the pore sizes of the binary and ternary composites with the HA compound, the pore sizes of both binary and ternary composites are larger than the HA compound. The more SF is added, the larger the pore size is formed, in contrast with a slightly decrease of the pore volume.

According to property requirements of the materials utilizing for bone filling, the obtained HA compound and the putty HA-based composites appear to be fine powder, with nanoscale size. The SF content in the composites decreases the pore volume but their porosity increases. Moreover, as RS played important role in improving the surface area, compressive strength, and Young's modulus of binary and tertiary HA-based composites, thus the putty composites can be applied for using as bone-filling materials. The main mechanical requirements of bone-filling material are shown in Table V.

As the values of the physical property's parameters of the natural bone and the prepared composites are compared, it is evidently seen that the properties of the prepared composites are similar to the natural bone. Therefore, this ternary HA/SF–RS composite can possibly be used as a bone replacement material. The usage of SF and RS organic phase from waste source materials and sol–gel method to produce HA-based composites has been proven to bring out the benefits from natural materials. In addition, this composite could be prepared without the addition of cross-linking agent, and low cost with uncomplicated technique.

CONCLUSIONS

The HA-based nanocomposites were successfully prepared using sol–gel method. The binary and ternary HA-based composites were obtained by the addition of SF and RS. The study on conformation of the HA-based composites showed that the SF and RS organic phase could be included homogenously in the crystal structure of HA composites. The prepared binary composite of HA/SF had a smaller crystallite size and less porosity than the HA/RS composite, but the addition of RS caused the increase in the compressive strength.

Upon preparing the ternary HA/SF–RS composites by adding 10% wt SF and 20% wt RS solution, the volume of each solution added were adjusted to study the effects on the composite's nanostructure. It was found that the addition of SF posed some effects as the SF content decreased, the number of pore and the porosity increased. On contrary, as the RS content increased, the lattice parameters, crystallinity, and crystallite size of the composites also increased which was agreeable with the increase of compressive strength and Young's modulus. The HA/SF-RS1 composites showed higher compressive strength (7.24 MPa) than the pure HA compound and modulus increased linearly with increase of RS content. The HA/SF–RS preparation pathway produced fine powder with nanoscale size. Moreover, RS also played an important role in improving the compressive strength and Young's modulus of HA/SF–RS composites. Hence this report shows the possibility of synthesizing the bone-filling

materials with enhanced fracture toughness. From such properties, the prepared HA/SF–RS composite should be tested further in an *in vivo* condition for using as bone-filling materials.

ACKNOWLEDGMENTS

Financial support from the Center of Excellence for Innovation in Chemistry (PERCH-CIC), Commission on Higher Education, Ministry of Education is gratefully acknowledged. Thanks also to the National Research University Project under Thailand's Office of Higher Education Commission (OHEC), Materials Science Research Center of the Faculty of Science and also the Graduate School, Chiang Mai University, for their partial financial supports.

REFERENCES

1. Dharap, P.; Li, Z. L.; Nagarajaiah, S.; Barrera, E. V. *Nanotechnology* **2004**, *15*(3), 379.
2. Chang, B. S.; Lee, C. K.; Hong, K. S.; Youn, H. J.; Ryu, H. S.; Chung, S. S.; Park, K. W. *Biomaterials* **2000**, *21*, 1291.
3. Altman, G. H.; Diaz, F.; Jakuba, C.; Calabro, T.; Horan, R. L.; Chen, J.; Lu, H.; Richmond, J.; Kaplan, D. L. *Biomaterials* **2003**, *24*, 401.
4. Wang, L.; Nemoto, R.; Senna, M. *J. Eur. Ceram. Soc.* **2004**, *24*, 2707.
5. Chunling, D.; Jin, J.; Li, Y.; Kong, X.; Wei, K.; Yao, J. *Mater. Sci. Eng. C* **2009**, *29*(1), 62.
6. Koonawoot, R.; Thiamsem, S.; Punyanitya, S.; Raksujarit, A.; Laosatirawong, S. *Chiang Mai Med. J.* **2010**, *49*(4), 139.
7. Sadjadi, M. S.; Meskinfam, M.; Jazdarreh, H. *Int. J. Nano. Dimens.* **2010**, *1*(1), 57.
8. Park, Y. T.; Kwon, K. J.; Park, Y. W.; Kim, S. G.; Kim, C. W.; Jo, Y. Y.; Kweon, H. Y.; Kang, S. W. *J. Korean Assoc. Maxillofac. Plast. Reconstr. Surg.* **2011**, *33*(6), 459.
9. Sriudom, S.; Niamsup, H.; Saipanya, S.; Watanesk, R.; Watanesk, S. *Appl. Mech. Mater.* **2014**, *446*, 408.
10. Moonsri, P.; Watanesk, R.; Watanesk, S.; Niamsup, H.; Deming, R. L. *J. Appl. Polym. Sci.* **2008**, *108*, 1402.
11. Goto, T.; Kim, I. Y.; Kikuta, K.; Ohtsuki, C. *Ceram. Int.* **2012**, *38*, 1003.
12. Zhang, H.; Zhang, M. *Ceram. Int.* **2011**, *37*, 279.
13. Simchuer, W.; Srisuwan, Y.; Baimark, Y.; Srihanam, P. *J. Biomater. Sci.* **2010**, *10*(5), 455.
14. Tongdeesoontorn, W.; Mauer, L. J.; Wongruong, S.; Sriburi, P.; Rachtanapun, P. *Chem. Cent. J.* **2011**, *5*, 1.
15. Bundela, H.; Bajpai, A. K. *eXPRESS Polym. Lett.* **2008**, *2*, 201.
16. Novitskaya, E.; Lee, S.; Lubarda, V. A.; McKittrick, J. *Acta Biomater.* **2012**, *8*, 1080.
17. Sallam, S. M.; Tohami, K. M.; Sallam, A. M.; Abo Salem, L. I.; Mohamed, F. A. *J. Biophys. Chem.* **2012**, *3*(4), 278.
18. Qin, Z.; Gautieri, A.; Nair, A. K.; Inbar, H.; Buehler, M. *J. Langmuir* **2012**, *28*, 1982.
19. Haider, A.; Gupta, K. C.; Kang, I.-K. *Nanoscale Res. Lett.* **2014**, *9*(314), 1.
20. Sanosh, K. P.; Chu, M.-C.; Balakrishnan, A.; Lee, Y.-J.; Kim, T. N.; Cho, S.-J. *Curr. Appl. Phys.* **2009**, *9*, 1459.
21. Fischer, H. R.; De Vlieger, J. J. In Handbook of Biodegradable Polymer Blends and Composites from Renewable Resources; Yu, L., Ed.; John Wiley & Sons, Inc.: New Jersey, **2009**; Part IV, p 269.
22. Tadic, D.; Epple, M. *Biomaterials* **2004**, *25*(6), 987.
23. Hing, K. A.; Best, S. M.; Tanner, K. E.; Bonfield, W.; Revell, P. A. *J. Biomed. Mater. Res. A* **2004**, *68*(1), 187.
24. Azami, M.; Samadikuchaksaraei, A.; Poursamar, S. A. *Int. J. Artif. Organs* **2010**, *33*(2), 86.
25. Manafi, S.; Rahimipour, M. R.; Yazdani, B.; Sadrnezhaad, S. K.; Amin, M. H.; *IJE Trans. B: Appl.* **2008**, *21*(2), 109.
26. Barralet, J. E.; Gaunt, T.; Wright, A. J.; Gibson, I. R.; Knowles, J. C. *J. Biomed. Mater. Res.* **2002**, *63*(1), 1.
27. Dudek, A.; Wlodarczyk, R. In Handbook of Ceramic Materials—Progress in Modern Ceramics; Feng, S., Ed.; InTech: Croatia, **2012**; Chapter 7, p 129.
28. Brostow, W.; Estevez, M.; Hagg, H.; Rodríguez, R.; Vargas, S. *J. Mater. Res.* **2008**, *23*, 1587.